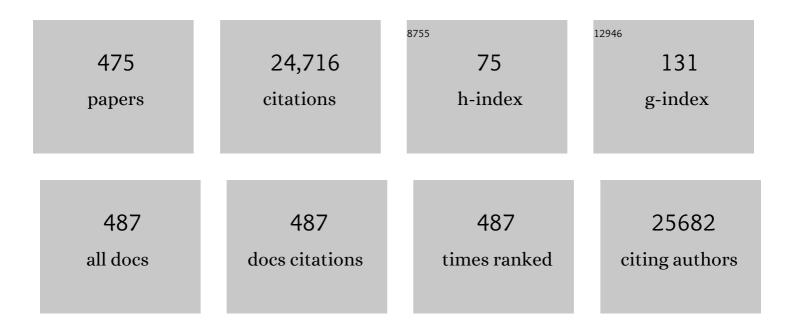
List of Publications by Year in descending order

Source: https://exaly.com/author-pdf/2951283/publications.pdf Version: 2024-02-01



FENC CHEN

#	Article	IF	CITATIONS
1	Isothermal Amplification of Nucleic Acids. Chemical Reviews, 2015, 115, 12491-12545.	47.7	1,292
2	Binary Strengthening and Toughening of MXene/Cellulose Nanofiber Composite Paper with Nacre-Inspired Structure and Superior Electromagnetic Interference Shielding Properties. ACS Nano, 2018, 12, 4583-4593.	14.6	942
3	Microwave-Assisted Preparation of Inorganic Nanostructures in Liquid Phase. Chemical Reviews, 2014, 114, 6462-6555.	47.7	688
4	Lightâ€Triggered Theranostics Based on Photosensitizerâ€Conjugated Carbon Dots for Simultaneous Enhancedâ€Fluorescence Imaging and Photodynamic Therapy. Advanced Materials, 2012, 24, 5104-5110.	21.0	630
5	Hollow/Rattle-Type Mesoporous Nanostructures by a Structural Difference-Based Selective Etching Strategy. ACS Nano, 2010, 4, 529-539.	14.6	615
6	Rattle-Structured Multifunctional Nanotheranostics for Synergetic Chemo-/Radiotherapy and Simultaneous Magnetic/Luminescent Dual-Mode Imaging. Journal of the American Chemical Society, 2013, 135, 6494-6503.	13.7	318
7	Dietary Modulation of Gut Microbiota Contributes to Alleviation of Both Genetic and Simple Obesity in Children. EBioMedicine, 2015, 2, 968-984.	6.1	306
8	The photoluminescence, drug delivery and imaging properties of multifunctional Eu3+/Gd3+ dual-doped hydroxyapatite nanorods. Biomaterials, 2011, 32, 9031-9039.	11.4	305
9	Ultrathin flexible reduced graphene oxide/cellulose nanofiber composite films with strongly anisotropic thermal conductivity and efficient electromagnetic interference shielding. Journal of Materials Chemistry C, 2017, 5, 3748-3756.	5.5	294
10	Ultrathin and Flexible CNTs/MXene/Cellulose Nanofibrils Composite Paper for Electromagnetic Interference Shielding. Nano-Micro Letters, 2019, 11, 72.	27.0	276
11	New Understanding in Tuning Toughness of β-Polypropylene: The Role of β-Nucleated Crystalline Morphology. Macromolecules, 2009, 42, 9325-9331.	4.8	274
12	Achieving a Collapsible, Strong, and Highly Thermally Conductive Film Based on Oriented Functionalized Boron Nitride Nanosheets and Cellulose Nanofiber. ACS Applied Materials & Interfaces, 2017, 9, 30035-30045.	8.0	258
13	The antifungal activity of graphene oxide–silver nanocomposites. Biomaterials, 2013, 34, 3882-3890.	11.4	249
14	MXeneâ€Reinforced Cellulose Nanofibril Inks for 3Dâ€Printed Smart Fibres and Textiles. Advanced Functional Materials, 2019, 29, 1905898.	14.9	206
15	Bioinspired Wetting Surface via Laser Microfabrication. ACS Applied Materials & Interfaces, 2013, 5, 6777-6792.	8.0	194
16	The resistivity–strain behavior of conductive polymer composites: stability and sensitivity. Journal of Materials Chemistry A, 2014, 2, 17085-17098.	10.3	185
17	A simple way to achieve superhydrophobicity, controllable water adhesion, anisotropic sliding, and anisotropic wetting based on femtosecond-laser-induced line-patterned surfaces. Journal of Materials Chemistry A, 2014, 2, 5499-5507.	10.3	172
18	Biocompatibility, MR imaging and targeted drug delivery of a rattle-type magnetic mesoporous silica nanosphere system conjugated with PEG and cancer-cell-specific ligands. Journal of Materials Chemistry, 2011, 21, 3037.	6.7	167

#	Article	IF	CITATIONS
19	Bioinspired Design of Underwater Superaerophobic and Superaerophilic Surfaces by Femtosecond Laser Ablation for Anti- or Capturing Bubbles. ACS Applied Materials & Interfaces, 2017, 9, 39863-39871.	8.0	162
20	Bioinspired underwater superoleophobic surface with ultralow oil-adhesion achieved by femtosecond laser microfabrication. Journal of Materials Chemistry A, 2014, 2, 8790-8795.	10.3	160
21	Direct Formation of Nanohybrid Shish-Kebab in the Injection Molded Bar of Polyethylene/Multiwalled Carbon Nanotubes Composite. Macromolecules, 2009, 42, 7016-7023.	4.8	159
22	Design and Preparation of a Unique Segregated Double Network with Excellent Thermal Conductive Property. ACS Applied Materials & amp; Interfaces, 2017, 9, 7637-7647.	8.0	155
23	Fire Alarm Wallpaper Based on Fire-Resistant Hydroxyapatite Nanowire Inorganic Paper and Graphene Oxide Thermosensitive Sensor. ACS Nano, 2018, 12, 3159-3171.	14.6	155
24	Highly Flexible and Nonflammable Inorganic Hydroxyapatite Paper. Chemistry - A European Journal, 2014, 20, 1242-1246.	3.3	152
25	Hydroxyapatite Hierarchically Nanostructured Porous Hollow Microspheres: Rapid, Sustainable Microwaveâ€Hydrothermal Synthesis by Using Creatine Phosphate as an Organic Phosphorus Source and Application in Drug Delivery and Protein Adsorption. Chemistry - A European Journal, 2013, 19, 5332-5341.	3.3	151
26	pHâ€Responsive Drugâ€Delivery Systems. Chemistry - an Asian Journal, 2015, 10, 284-305.	3.3	150
27	Remarkably simple achievement of superhydrophobicity, superhydrophilicity, underwater superoleophobicity, underwater superoleophilicity, underwater superaerophobicity, and underwater superaerophilicity on femtosecond laser ablated PDMS surfaces. Journal of Materials Chemistry A, 2017. 5. 25249-25257.	10.3	147
28	A Stretchable Highoutput Triboelectric Nanogenerator Improved by MXene Liquid Electrode with High Electronegativity. Advanced Functional Materials, 2020, 30, 2004181.	14.9	147
29	Wearable, ultrathin and transparent bacterial celluloses/MXene film with Janus structure and excellent mechanical property for electromagnetic interference shielding. Chemical Engineering Journal, 2021, 403, 126438.	12.7	145
30	Femtosecond Laser Weaving Superhydrophobic Patterned PDMS Surfaces with Tunable Adhesion. Journal of Physical Chemistry C, 2013, 117, 24907-24912.	3.1	143
31	Hierachically Nanostructured Mesoporous Spheres of Calcium Silicate Hydrate: Surfactantâ€Free Sonochemical Synthesis and Drugâ€Đelivery System with Ultrahigh Drug‣oading Capacity. Advanced Materials, 2010, 22, 749-753.	21.0	142
32	Simultaneous nuclear imaging and intranuclear drug delivery by nuclear-targeted multifunctional upconversion nanoprobes. Biomaterials, 2012, 33, 7282-7290.	11.4	139
33	Largely enhanced energy storage density of poly(vinylidene fluoride) nanocomposites based on surface hydroxylation of boron nitride nanosheets. Journal of Materials Chemistry A, 2018, 6, 7573-7584.	10.3	139
34	Maskless fabrication of concave microlens arrays on silica glasses by a femtosecond-laser-enhanced local wet etching method. Optics Express, 2010, 18, 20334.	3.4	138
35	Fabrication of a transparent superamphiphobic coating with improved stability. Soft Matter, 2011, 7, 6435.	2.7	137
36	Preparation of polyester/reduced graphene oxide composites via in situ melt polycondensation and simultaneous thermo-reduction of graphene oxide. Journal of Materials Chemistry, 2011, 21, 8612.	6.7	137

#	Article	IF	CITATIONS
37	Two-dimensional MXene-reinforced robust surface superhydrophobicity with self-cleaning and photothermal-actuating binary effects. Materials Horizons, 2019, 6, 1057-1065.	12.2	135
38	Hydroxyapatite nanosheet-assembled porous hollow microspheres: DNA-templated hydrothermal synthesis, drug delivery and protein adsorption. Journal of Materials Chemistry, 2012, 22, 22642.	6.7	134
39	Robust and Mechanically and Electrically Self-Healing Hydrogel for Efficient Electromagnetic Interference Shielding. ACS Applied Materials & Interfaces, 2018, 10, 8245-8257.	8.0	134
40	Sol–Gel Synthesis of Metal–Phenolic Coordination Spheres and Their Derived Carbon Composites. Angewandte Chemie - International Edition, 2018, 57, 9838-9843.	13.8	127
41	Highly Stable Amorphous Calcium Phosphate Porous Nanospheres: Microwaveâ€Assisted Rapid Synthesis Using ATP as Phosphorus Source and Stabilizer, and Their Application in Anticancer Drug Delivery. Chemistry - A European Journal, 2013, 19, 981-987.	3.3	125
42	Femtosecond laser controlled wettability of solid surfaces. Soft Matter, 2015, 11, 8897-8906.	2.7	125
43	Ultrasound-assisted biosynthesis of CuO-NPs using brown alga Cystoseira trinodis: Characterization, photocatalytic AOP, DPPH scavenging and antibacterial investigations. Ultrasonics Sonochemistry, 2018, 41, 109-119.	8.2	125
44	Multifunctional Eu3+/Gd3+ dual-doped calcium phosphate vesicle-like nanospheres for sustained drug release and imaging. Biomaterials, 2012, 33, 6447-6455.	11.4	122
45	Photoinduced switchable underwater superoleophobicity–superoleophilicity on laser modified titanium surfaces. Journal of Materials Chemistry A, 2015, 3, 10703-10709.	10.3	122
46	Oilâ€Water Separation: A Gift from the Desert. Advanced Materials Interfaces, 2016, 3, 1500650.	3.7	121
47	<i>Nepenthes</i> Inspired Design of Selfâ€Repairing Omniphobic Slippery Liquid Infused Porous Surface (SLIPS) by Femtosecond Laser Direct Writing. Advanced Materials Interfaces, 2017, 4, 1700552.	3.7	120
48	Preparation of a thermally conductive biodegradable cellulose nanofiber/hydroxylated boron nitride nanosheet film: the critical role of edge-hydroxylation. Journal of Materials Chemistry A, 2018, 6, 11863-11873.	10.3	119
49	Large-Scale Automated Production of Highly Ordered Ultralong Hydroxyapatite Nanowires and Construction of Various Fire-Resistant Flexible Ordered Architectures. ACS Nano, 2016, 10, 11483-11495.	14.6	114
50	Bioinspired Ultralight Inorganic Aerogel for Highly Efficient Air Filtration and Oil–Water Separation. ACS Applied Materials & Interfaces, 2018, 10, 13019-13027.	8.0	112
51	Co-precipitation synthesis route to yttrium aluminum garnet (YAC) transparent ceramics. Journal of the European Ceramic Society, 2012, 32, 2971-2979.	5.7	110
52	Fabricating MnO ₂ Nanozymes as Intracellular Catalytic DNA Circuit Generators for Versatile Imaging of Baseâ€Excision Repair in Living Cells. Advanced Functional Materials, 2017, 27, 1702748.	14.9	106
53	Phase change material with anisotropically high thermal conductivity and excellent shape stability due to its robust cellulose/BNNSs skeleton. Journal of Materials Chemistry A, 2019, 7, 19364-19373.	10.3	103
54	Biomimetic hydroxyapatite porous microspheres with co-substituted essential trace elements: Surfactant-free hydrothermal synthesis, enhanced degradation and drug release. Journal of Materials Chemistry, 2011, 21, 16558.	6.7	102

#	Article	IF	CITATIONS
55	Dragonflyâ€Eyeâ€Inspired Artificial Compound Eyes with Sophisticated Imaging. Advanced Functional Materials, 2016, 26, 1995-2001.	14.9	102
56	Bioinspired transparent underwater superoleophobic and anti-oil surfaces. Journal of Materials Chemistry A, 2015, 3, 9379-9384.	10.3	99
57	Target-Triggered Three-Way Junction Structure and Polymerase/Nicking Enzyme Synergetic Isothermal Quadratic DNA Machine for Highly Specific, One-Step, and Rapid MicroRNA Detection at Attomolar Level. Analytical Chemistry, 2014, 86, 8098-8105.	6.5	98
58	A Review of Femtosecondâ€Laserâ€Induced Underwater Superoleophobic Surfaces. Advanced Materials Interfaces, 2018, 5, 1701370.	3.7	95
59	3D Silver Nanoparticles Decorated Zinc Oxide/Silicon Heterostructured Nanomace Arrays as High-Performance Surface-Enhanced Raman Scattering Substrates. ACS Applied Materials & Interfaces, 2015, 7, 5725-5735.	8.0	93
60	Calcium phosphate-phosphorylated adenosine hybrid microspheres for anti-osteosarcoma drug delivery and osteogenic differentiation. Biomaterials, 2017, 121, 1-14.	11.4	93
61	Completely Green Approach for the Preparation of Strong and Highly Conductive Graphene Composite Film by Using Nanocellulose as Dispersing Agent and Mechanical Compression. ACS Sustainable Chemistry and Engineering, 2017, 5, 9102-9113.	6.7	90
62	Programming Enzyme-Initiated Autonomous DNAzyme Nanodevices in Living Cells. ACS Nano, 2017, 11, 11908-11914.	14.6	89
63	A review of femtosecond laser-structured superhydrophobic or underwater superoleophobic porous surfaces/materials for efficient oil/water separation. RSC Advances, 2019, 9, 12470-12495.	3.6	89
64	Nucleic Acids Analysis. Science China Chemistry, 2021, 64, 171-203.	8.2	88
65	Synthesis of La3+ doped mesoporous titania with highly crystallized walls. Microporous and Mesoporous Materials, 2005, 79, 93-99.	4.4	87
66	Highly sensitive fluorescence assay of DNA methyltransferase activity via methylation-sensitive cleavage coupled with nicking enzyme-assisted signalamplification. Biosensors and Bioelectronics, 2013, 42, 56-61.	10.1	87
67	Nanosheet-assembled hierarchical nanostructures of hydroxyapatite: surfactant-free microwave-hydrothermal rapid synthesis, protein/DNA adsorption and pH-controlled release. CrystEngComm, 2013, 15, 206-212.	2.6	86
68	Femtosecond Laser Direct Writing of Porous Network Microstructures for Fabricating Superâ€Slippery Surfaces with Excellent Liquid Repellence and Anti ell Proliferation. Advanced Materials Interfaces, 2018, 5, 1701479.	3.7	86
69	Study on structural changes of microwave heat-moisture treated resistant Canna edulis Ker starch during digestion in vitro. Food Hydrocolloids, 2010, 24, 27-34.	10.7	85
70	Microwave-assisted hydrothermal rapid synthesis of hydroxyapatite nanowires using adenosine 5'-triphosphate disodium salt as phosphorus source. Materials Letters, 2012, 85, 71-73.	2.6	85
71	Surfactant-free solvothermal synthesis of hydroxyapatite nanowire/nanotube ordered arrays with biomimetic structures. CrystEngComm, 2011, 13, 1858-1863.	2.6	84
72	Surface modifications of boron nitride nanosheets for poly(vinylidene fluoride) based film capacitors: advantages of edge-hydroxylation. Journal of Materials Chemistry A, 2019, 7, 7664-7674.	10.3	82

#	Article	IF	CITATIONS
73	Electrospun chitosan-P(LLA-CL) nanofibers for biomimetic extracellular matrix. Journal of Biomaterials Science, Polymer Edition, 2008, 19, 677-691.	3.5	80
74	Green in Situ Synthesis of Clean 3D Chestnutlike Ag/WO _{3–<i>x</i>} Nanostructures for Highly Efficient, Recyclable and Sensitive SERS Sensing. ACS Applied Materials & Interfaces, 2017, 9, 7436-7446.	8.0	80
75	Intracellular Entropyâ€Driven Multiâ€Bit DNA Computing for Tumor Progression Discrimination. Angewandte Chemie - International Edition, 2020, 59, 13267-13272.	13.8	80
76	Prognostic value of immune checkpoint molecules in breast cancer. Bioscience Reports, 2020, 40, .	2.4	80
77	Amorphous calcium phosphate, hydroxyapatite and poly(d , l -lactic acid) composite nanofibers: Electrospinning preparation, mineralization and in vivo bone defect repair. Colloids and Surfaces B: Biointerfaces, 2015, 136, 27-36.	5.0	79
78	Hydroxyapatite nanosheet-assembled microspheres: Hemoglobin-templated synthesis and adsorption for heavy metal ions. Journal of Colloid and Interface Science, 2014, 416, 11-18.	9.4	78
79	Europium-doped amorphous calcium phosphate porous nanospheres: preparation and application as luminescent drug carriers. Nanoscale Research Letters, 2011, 6, 67.	5.7	77
80	Hydrophobic cellulose films with excellent strength and toughness via ball milling activated acylation of microfibrillated cellulose. Carbohydrate Polymers, 2016, 154, 129-138.	10.2	76
81	Chitosan-coated mesoporous microspheres of calcium silicate hydrate: Environmentally friendly synthesis and application as a highly efficient adsorbent for heavy metal ions. Journal of Colloid and Interface Science, 2014, 418, 208-215.	9.4	75
82	Dependence of mechanical properties on βâ€form content and crystalline morphology for βâ€nucleated isotactic polypropylene. Polymers for Advanced Technologies, 2011, 22, 2044-2054.	3.2	74
83	Cardioprotective mechanism of SGLT2 inhibitor against myocardial infarction is through reduction of autosis. Protein and Cell, 2022, 13, 336-359.	11.0	74
84	Hydroxyapatite nanorods/poly(vinyl pyrolidone) composite nanofibers, arrays and three-dimensional fabrics: Electrospun preparation and transformation to hydroxyapatite nanostructures. Acta Biomaterialia, 2010, 6, 3013-3020.	8.3	73
85	Microwave Hydrothermal Transformation of Amorphous Calcium Carbonate Nanospheres and Application in Protein Adsorption. ACS Applied Materials & Interfaces, 2014, 6, 4310-4320.	8.0	72
86	<p>Engineering of Aerogel-Based Biomaterials for Biomedical Applications</p> . International Journal of Nanomedicine, 2020, Volume 15, 2363-2378.	6.7	72
87	Control of the hierarchical structure of polymer articles via "structuring―processing. Progress in Polymer Science, 2014, 39, 891-920.	24.7	71
88	Solvothermal synthesis of submillimeter ultralong hydroxyapatite nanowires using a calcium oleate precursor in a series of monohydroxy alcohols. Ceramics International, 2015, 41, 6098-6102.	4.8	71
89	Silicone-Coated MXene/Cellulose Nanofiber Aerogel Films with Photothermal and Joule Heating Performances for Electromagnetic Interference Shielding. ACS Applied Nano Materials, 2021, 4, 7234-7243.	5.0	71
90	Flower‣ike Hierarchically Nanostructured Hydroxyapatite Hollow Spheres: Facile Preparation and Application in Anticancer Drug Cellular Delivery. Chemistry - an Asian Journal, 2010, 5, 2477-2482.	3.3	70

#	Article	IF	CITATIONS
91	A methylation-blocked cascade amplification strategy for label-free colorimetric detection of DNA methyltransferase activity. Biosensors and Bioelectronics, 2014, 54, 565-570.	10.1	70
92	Enhanced osteogenesis and angiogenesis by mesoporous hydroxyapatite microspheres-derived simvastatin sustained release system for superior bone regeneration. Scientific Reports, 2017, 7, 44129.	3.3	70
93	Comparative study of porous hydroxyapatite/chitosan and whitlockite/chitosan scaffolds for bone regeneration in calvarial defects. International Journal of Nanomedicine, 2017, Volume 12, 2673-2687.	6.7	69
94	Photo-Fenton degradation of malachite green catalyzed by aromatic compounds under visible light irradiation. New Journal of Chemistry, 2002, 26, 336-341.	2.8	67
95	Influence of electronic effects from bridging groups on synthetic reaction and thermally activated polymerization of bisphenolâ€based benzoxazines. Journal of Polymer Science Part A, 2011, 49, 1443-1452.	2.3	67
96	Systemic and cerebral exposure to and pharmacokinetics of flavonols and terpene lactones after dosing standardized <i><scp>G</scp>inkgo biloba</i> leaf extracts to rats via different routes of administration. British Journal of Pharmacology, 2013, 170, 440-457.	5.4	67
97	A novel lncRNA‣INC01116 regulates tumorigenesis of glioma by targeting VEGFA. International Journal of Cancer, 2020, 146, 248-261.	5.1	67
98	Synthesis, Structural Characterizations and Magnetic Properties of a Series of Mono-, Di- and Polynuclear Manganese Pyridinecarboxylate Compounds. European Journal of Inorganic Chemistry, 2004, 2004, 1454-1464.	2.0	66
99	Hydrothermal synthesis of hydroxyapatite nanorods and nanowires using riboflavin-5′-phosphate monosodium salt as a new phosphorus source and their application in protein adsorption. CrystEngComm, 2013, 15, 7926.	2.6	66
100	Ultrathin Calcium Silicate Hydrate Nanosheets with Large Specific Surface Areas: Synthesis, Crystallization, Layered Selfâ€Assembly and Applications as Excellent Adsorbents for Drug, Protein, and Metal Ions. Small, 2013, 9, 2911-2925.	10.0	66
101	Strontium-Doped Amorphous Calcium Phosphate Porous Microspheres Synthesized through a Microwave-Hydrothermal Method Using Fructose 1,6-Bisphosphate as an Organic Phosphorus Source: Application in Drug Delivery and Enhanced Bone Regeneration. ACS Applied Materials & Martials & Martiales, 2017, 9, 3306-3317.	8.0	66
102	Mechanically Strong Chitin Fibers with Nanofibril Structure, Biocompatibility, and Biodegradability. Chemistry of Materials, 2019, 31, 2078-2087.	6.7	66
103	Chiral guanosine 5′-monophosphate-capped gold nanoflowers: Controllable synthesis, characterization, surface-enhanced Raman scattering activity, cellular imaging and photothermal therapy. Nano Research, 2012, 5, 630-639.	10.4	65
104	Superior strength and highly thermoconductive cellulose/ boron nitride film by stretch-induced alignment. Journal of Materials Chemistry A, 2021, 9, 10304-10315.	10.3	65
105	The preparation and properties of polystyrene/functionalized graphene nanocomposite foams using supercritical carbon dioxide. Polymer International, 2013, 62, 1077-1084.	3.1	64
106	Single copy-sensitive electrochemical assay for circulating methylated DNA in clinical samples with ultrahigh specificity based on a sequential discrimination–amplification strategy. Chemical Science, 2017, 8, 4764-4770.	7.4	64
107	Substrate-Independent, Fast, and Reversible Switching between Underwater Superaerophobicity and Aerophilicity on the Femtosecond Laser-Induced Superhydrophobic Surfaces for Selectively Repelling or Capturing Bubbles in Water. ACS Applied Materials & amp; Interfaces, 2019, 11, 8667-8675.	8.0	64

108 Title is missing!. Catalysis Letters, 1999, 58, 245-247.

2.6 63

#	Article	IF	CITATIONS
109	Cross-Linking of Gelatin and Chitosan Complex Nanofibers for Tissue-Engineering Scaffolds. Journal of Biomaterials Science, Polymer Edition, 2011, 22, 1099-1113.	3.5	63
110	Fabrication of through holes in silicon carbide using femtosecond laser irradiation and acid etching. Applied Surface Science, 2014, 289, 529-532.	6.1	61
111	Green, Biodegradable, Underwater Superoleophobic Wood Sheet for Efficient Oil/Water Separation. ACS Omega, 2018, 3, 1395-1402.	3.5	61
112	Green Production of Regenerated Cellulose/Boron Nitride Nanosheet Textiles for Static and Dynamic Personal Cooling. ACS Applied Materials & Interfaces, 2019, 11, 40685-40693.	8.0	61
113	DNA Triplex and Quadruplex Assembled Nanosensors for Correlating K ⁺ and pH in Lysosomes. Angewandte Chemie - International Edition, 2021, 60, 5453-5458.	13.8	61
114	Calcium phosphate/PLGA-mPEG hybrid porous nanospheres: A promising vector with ultrahigh gene loading and transfection efficiency. Journal of Materials Chemistry, 2010, 20, 1161-1166.	6.7	60
115	Highly sensitive detection of telomerase activity in tumor cells by cascade isothermal signal amplification based on three-way junction and base-stacking hybridization. Biosensors and Bioelectronics, 2013, 41, 764-770.	10.1	60
116	Stable superhydrophobic surface with hierarchical mesh-porous structure fabricated by a femtosecond laser. Applied Physics A: Materials Science and Processing, 2013, 111, 243-249.	2.3	60
117	Reversible Underwater Lossless Oil Droplet Transportation. Advanced Materials Interfaces, 2015, 2, 1400388.	3.7	60
118	Preparation and enhanced mechanical properties of hybrid hydrogels comprising ultralong hydroxyapatite nanowires and sodium alginate. Journal of Colloid and Interface Science, 2017, 497, 266-275.	9.4	60
119	Hydroxyapatite Nanowire@Magnesium Silicate Core–Shell Hierarchical Nanocomposite: Synthesis and Application in Bone Regeneration. ACS Applied Materials & Interfaces, 2017, 9, 16435-16447.	8.0	60
120	Polydopamine@Gold Nanowaxberry Enabling Improved SERS Sensing of Pesticides, Pollutants, and Explosives in Complex Samples. Analytical Chemistry, 2018, 90, 9048-9054.	6.5	60
121	Polyhedral Oligomeric Silsesquioxanes Based Ultralowâ€ <i>k</i> Materials: The Effect of Cage Size. Advanced Functional Materials, 2021, 31, 2102074.	14.9	60
122	A promising alternative to conventional polyethylene with poly(propylene carbonate) reinforced by graphene oxide nanosheets. Journal of Materials Chemistry, 2011, 21, 17627.	6.7	58
123	Hierarchical Hollow Hydroxyapatite Microspheres: Microwaveâ€Assisted Rapid Synthesis by Using Pyridoxalâ€5′â€₽hosphate as a Phosphorus Source and Application in Drug Delivery. Chemistry - an Asian Journal, 2013, 8, 1313-1320.	3.3	58
124	Hydrothermal syntheses, crystal structures and luminescent properties of zinc(II) coordination polymers constructed by bifunctional tetrazolate-5-carboxylate ligands. CrystEngComm, 2010, 12, 260-269.	2.6	57
125	Ultralong hydroxyapatite nanowires synthesized by solvothermal treatment using a series of phosphate sodium salts. Materials Letters, 2015, 144, 135-137.	2.6	57
126	Hydroxylapatite nanorods: An efficient and promising carrier for gene transfection. Journal of Colloid and Interface Science, 2010, 345, 427-432.	9.4	56

#	Article	IF	CITATIONS
127	Copper-doped mesoporous hydroxyapatite microspheres synthesized by a microwave-hydrothermal method using creatine phosphate as an organic phosphorus source: application in drug delivery and enhanced bone regeneration. Journal of Materials Chemistry B, 2017, 5, 1039-1052.	5.8	56
128	Mechanically Strong Multifilament Fibers Spun from Cellulose Solution via Inducing Formation of Nanofibers. ACS Sustainable Chemistry and Engineering, 2018, 6, 5314-5321.	6.7	56
129	Smart photocatalytic removal of ammonia through molecular recognition of zinc ferrite/reduced graphene oxide hybrid catalyst under visible-light irradiation. Catalysis Science and Technology, 2017, 7, 3210-3219.	4.1	55
130	Amorphous calcium phosphate/poly(d,l-lactic acid) composite nanofibers: Electrospinning preparation and biomineralization. Journal of Colloid and Interface Science, 2011, 359, 371-379.	9.4	54
131	Mismatch Extension of DNA Polymerases and High-Accuracy Single Nucleotide Polymorphism Diagnostics by Gold Nanoparticle-Improved Isothermal Amplification. Analytical Chemistry, 2015, 87, 8718-8723.	6.5	54
132	α-Fe 2 O 3 nanosheet-assembled hierarchical hollow mesoporous microspheres: Microwave-assisted solvothermal synthesis and application in photocatalysis. Journal of Colloid and Interface Science, 2016, 463, 107-117.	9.4	54
133	Hydroxyapatite Nanowire-Based All-Weather Flexible Electrically Conductive Paper with Superhydrophobic and Flame-Retardant Properties. ACS Applied Materials & Interfaces, 2017, 9, 39534-39548.	8.0	54
134	Compressed Ultrafast Spectral-Temporal Photography. Physical Review Letters, 2019, 122, 193904.	7.8	54
135	Microwave-assisted synthesis of hydroxyapatite hollow microspheres in aqueous solution. Materials Letters, 2011, 65, 2361-2363.	2.6	53
136	Porous hollow microspheres of amorphous calcium phosphate: soybean lecithin templated microwave-assisted hydrothermal synthesis and application in drug delivery. Journal of Materials Chemistry B, 2015, 3, 1823-1830.	5.8	53
137	Design of a novel wound dressing consisting of alginate hydrogel and simvastatin-incorporated mesoporous hydroxyapatite microspheres for cutaneous wound healing. RSC Advances, 2016, 6, 104375-104387.	3.6	53
138	Towards high-performance poly(<scp>l</scp> -lactide)/elastomer blends with tunable interfacial adhesion and matrix crystallization via constructing stereocomplex crystallites at the interface. RSC Advances, 2014, 4, 49374-49385.	3.6	52
139	Highly Flexible Multifunctional Biopaper Comprising Chitosan Reinforced by Ultralong Hydroxyapatite Nanowires. Chemistry - A European Journal, 2017, 23, 3850-3862.	3.3	52
140	Magnetic nanocomposite of hydroxyapatite ultrathin nanosheets/Fe3O4 nanoparticles: microwave-assisted rapid synthesis and application in pH-responsive drug release. Biomaterials Science, 2013, 1, 1074.	5.4	51
141	Multifunctional Calcium Phosphate Nanostructured Materials and Biomedical Applications. Current Nanoscience, 2014, 10, 465-485.	1.2	51
142	Fructose 1,6â€Bisphosphate Trisodium Salt as A New Phosphorus Source for the Rapid Microwave Synthesis of Porous Calcium–Phosphate Microspheres and their Application in Drug Delivery. Chemistry - an Asian Journal, 2013, 8, 88-94.	3.3	50
143	Nature-Inspired Superwettability Achieved by Femtosecond Lasers. Ultrafast Science, 2022, 2022, .	11.2	50
144	Mutual wetting transition between isotropic and anisotropic on directional structures fabricated by femotosecond laser. Soft Matter, 2011, 7, 8337.	2.7	49

#	Article	IF	CITATIONS
145	Electrospinning of PELA/PPY Fibrous Conduits: Promoting Peripheral Nerve Regeneration in Rats by Self-Originated Electrical Stimulation. ACS Biomaterials Science and Engineering, 2016, 2, 1572-1581.	5.2	49
146	Fabrication of bioinspired omnidirectional and gapless microlens array for wide field-of-view detections. Applied Physics Letters, 2012, 100, .	3.3	48
147	Hierarchical Assembly of Monodisperse Hydroxyapatite Nanowires and Construction of Highâ€Strength Fireâ€Resistant Inorganic Paper with Highâ€Temperature Flexibility. ChemNanoMat, 2017, 3, 259-268.	2.8	48
148	Bioinspired Fabrication of Bi/Tridirectionally Anisotropic Sliding Superhydrophobic PDMS Surfaces by Femtosecond Laser. Advanced Materials Interfaces, 2018, 5, 1701245.	3.7	48
149	Enhanced Photocatalytic H ₂ Production on Three-Dimensional Porous CeO ₂ /Carbon Nanostructure. ACS Sustainable Chemistry and Engineering, 2018, 6, 9691-9698.	6.7	48
150	How To Obtain Six Different Superwettabilities on a Same Microstructured Pattern: Relationship between Various Superwettabilities in Different Solid/Liquid/Gas Systems. Langmuir, 2019, 35, 921-927.	3.5	48
151	Designing "Supermetalphobic―Surfaces that Greatly Repel Liquid Metal by Femtosecond Laser Processing: Does the Surface Chemistry or Microstructure Play a Crucial Role?. Advanced Materials Interfaces, 2020, 7, 1901931.	3.7	48
152	Zinc(II) and Cadmium(II) Coordination Polymers Based on 3â€(5 <i>H</i> â€Tetrazolyl)benzoate Ligand with Different Coordination Modes: Hydrothermal Syntheses, Crystal Structures and Ligandâ€Centered Luminescence. European Journal of Inorganic Chemistry, 2010, 2010, 4982-4991.	2.0	47
153	Calcium phosphate drug nanocarriers with ultrahigh and adjustable drug-loading capacity: One-step synthesis, in situ drug loading and prolonged drug release. Nanomedicine: Nanotechnology, Biology, and Medicine, 2011, 7, 428-434.	3.3	47
154	Methylation-blocked enzymatic recycling amplification for highly sensitive fluorescence sensing of DNA methyltransferase activity. Analyst, The, 2013, 138, 284-289.	3.5	47
155	Influences of Coagulation Conditions on the Structure and Properties of Regenerated Cellulose Filaments via Wet-Spinning in LiOH/Urea Solvent. ACS Sustainable Chemistry and Engineering, 2018, 6, 4056-4067.	6.7	47
156	Photochemical synthesis of ZnO@Au nanorods as an advanced reusable SERS substrate for ultrasensitive detection of light-resistant organic pollutant in wastewater. Talanta, 2019, 194, 680-688.	5.5	47
157	Amplified fluorescence detection of mercury(ii) ions (Hg2+) using target-induced DNAzyme cascade with catalytic and molecular beacons. Analyst, The, 2012, 137, 2799.	3.5	46
158	Multifunctional biodegradable mesoporous microspheres of Eu ³⁺ -doped amorphous calcium phosphate: microwave-assisted preparation, pH-sensitive drug release, and bioimaging application. Journal of Materials Chemistry B, 2014, 2, 7132-7140.	5.8	46
159	Programming <i>in situ</i> accelerated DNA walkers in diffusion-limited microenvironments. Chemical Science, 2019, 10, 3103-3109.	7.4	46
160	Gasdermin D inhibition confers antineutrophil-mediated cardioprotection in acute myocardial infarction. Journal of Clinical Investigation, 2022, 132, .	8.2	46
161	Synthesis, Structure and Magnetic Properties of a Series of Novel Isophthalate-Bridged Manganese(II) Polymers with Double-Layer or Double-Chain Structures. European Journal of Inorganic Chemistry, 2004, 2004, 3316-3325.	2.0	45
162	Genotyping of human papillomavirus in cervical lesions by L1 consensus PCR and the Luminex xMAP system. Journal of Medical Microbiology, 2006, 55, 715-720.	1.8	45

#	Article	IF	CITATIONS
163	Rodent stroke induced by photochemical occlusion of proximal middle cerebral artery: Evolution monitored with MR imaging and histopathology. European Journal of Radiology, 2007, 63, 68-75.	2.6	45
164	Amorphous calcium silicate hydrate/block copolymer hybrid nanoparticles: synthesis and application as drug carriers. Dalton Transactions, 2013, 42, 7032.	3.3	45
165	MnO ₂ -Nanosheet-Powered Protective Janus DNA Nanomachines Supporting Robust RNA Imaging. Analytical Chemistry, 2018, 90, 2271-2276.	6.5	45
166	Bioinspired MXene-Based User-Interactive Electronic Skin for Digital and Visual Dual-Channel Sensing. Nano-Micro Letters, 2022, 14, 119.	27.0	45
167	Bioinspired superhydrophobic surfaces with directional Adhesion. RSC Advances, 2014, 4, 8138.	3.6	44
168	Ag Nanoparticles Decorated Cactus-Like Ag Dendrites/Si Nanoneedles as Highly Efficient 3D Surface-Enhanced Raman Scattering Substrates toward Sensitive Sensing. Analytical Chemistry, 2015, 87, 10527-10534.	6.5	44
169	Accurate Electrochemistry Analysis of Circulating Methylated DNA from Clinical Plasma Based on Paired-End Tagging and Amplifications. Analytical Chemistry, 2017, 89, 10468-10473.	6.5	44
170	Strong and Highly Conductive Graphene Composite Film Based on the Nanocellulose-Assisted Dispersion of Expanded Graphite and Incorporation of Poly(ethylene oxide). ACS Sustainable Chemistry and Engineering, 2019, 7, 5045-5056.	6.7	43
171	DNA Triplex and Quadruplex Assembled Nanosensors for Correlating K + and pH in Lysosomes. Angewandte Chemie, 2021, 133, 5513-5518.	2.0	43
172	The study on the degradation and mineralization mechanism of ionâ€doped calcium polyphosphate <i>in vitro</i> . Journal of Biomedical Materials Research - Part B Applied Biomaterials, 2009, 89B, 430-438.	3.4	42
173	Porous microspheres of magnesium whitlockite and amorphous calcium magnesium phosphate: microwave-assisted rapid synthesis using creatine phosphate, and application in drug delivery. Journal of Materials Chemistry B, 2015, 3, 7775-7786.	5.8	42
174	Synthesis and Characterization of Magnetic Iron Oxide/Calcium Silicate Mesoporous Nanocomposites as a Promising Vehicle for Drug Delivery. ACS Applied Materials & Interfaces, 2012, 4, 6969-6974.	8.0	41
175	One-step highly sensitive florescence detection of T4 polynucleotide kinase activity and biological small molecules by ligation-nicking coupled reaction-mediated signal amplification. Biosensors and Bioelectronics, 2013, 47, 218-224.	10.1	41
176	ATPâ€Stabilized Amorphous Calcium Carbonate Nanospheres and Their Application in Protein Adsorption. Small, 2014, 10, 2047-2056.	10.0	41
177	Ultralong Hydroxyapatite Nanowire/Collagen Biopaper with High Flexibility, Improved Mechanical Properties and Excellent Cellular Attachment. Chemistry - an Asian Journal, 2017, 12, 655-664.	3.3	41
178	Biocompatible, Ultralight, Strong Hydroxyapatite Networks Based on Hydroxyapatite Microtubes with Excellent Permeability and Ultralow Thermal Conductivity. ACS Applied Materials & Interfaces, 2017, 9, 7918-7928.	8.0	41
179	Tumor resistance to vascular disrupting agents: mechanisms, imaging, and solutions. Oncotarget, 2016, 7, 15444-15459.	1.8	41
180	Mechanically reinforced chitosan/cellulose nanocrystals composites with good transparency and biocompatibility. Chinese Journal of Polymer Science (English Edition), 2015, 33, 61-69.	3.8	40

#	Article	IF	CITATIONS
181	Porous microspheres of amorphous calcium phosphate: Block copolymer templated microwave-assisted hydrothermal synthesis and application in drug delivery. Journal of Colloid and Interface Science, 2015, 443, 72-79.	9.4	40
182	Preparation of polyvinylidene fluoride/expanded graphite composites with enhanced thermal conductivity via ball milling treatment. RSC Advances, 2016, 6, 45578-45584.	3.6	40
183	Sonochemical synthesis of hydroxyapatite nanoflowers using creatine phosphate disodium salt as an organic phosphorus source and their application in protein adsorption. RSC Advances, 2016, 6, 9686-9692.	3.6	40
184	Solvothermal synthesis of oriented hydroxyapatite nanorod/nanosheet arrays using creatine phosphate as phosphorus source. CrystEngComm, 2013, 15, 4527.	2.6	39
185	Adsorption and Synergetic Fenton-like Degradation of Methylene Blue by a Novel Mesoporous α-Fe ₂ O ₃ /SiO ₂ at Neutral pH. Industrial & Engineering Chemistry Research, 2018, 57, 5539-5549.	3.7	39
186	Sol–Gel Synthesis of Metal–Phenolic Coordination Spheres and Their Derived Carbon Composites. Angewandte Chemie, 2018, 130, 9986-9991.	2.0	39
187	Rapid microwave-assisted synthesis and characterization of cellulose-hydroxyapatite nanocomposites in N,N-dimethylacetamide solvent. Carbohydrate Research, 2010, 345, 1046-1050.	2.3	38
188	Amorphous calcium phosphate nanospheres/polylactide composite coated tantalum scaffold: Facile preparation, fast biomineralization and subchondral bone defect repair application. Colloids and Surfaces B: Biointerfaces, 2014, 123, 236-245.	5.0	38
189	Vesicle-like nanospheres of amorphous calcium phosphate: sonochemical synthesis using the adenosine 5′-triphosphate disodium salt and their application in pH-responsive drug delivery. Journal of Materials Chemistry B, 2015, 3, 7347-7354.	5.8	38
190	Femtosecond laser preparing patternable liquid-metal-repellent surface for flexible electronics. Journal of Colloid and Interface Science, 2020, 578, 146-154.	9.4	38
191	Porous nanocomposites of PEG-PLA/calcium phosphate: room-temperature synthesis and its application in drug delivery. Dalton Transactions, 2010, 39, 4435.	3.3	37
192	Microwave-assisted rapid synthesis and photocatalytic activity of mesoporous Nd-doped SrTiO3 nanospheres and nanoplates. Materials Letters, 2013, 100, 62-65.	2.6	37
193	Solvothermal synthesis of hydroxyapatite nanostructures with various morphologies using adenosine 5′-monophosphate sodium salt as an organic phosphorus source. RSC Advances, 2015, 5, 3792-3798.	3.6	37
194	Tunable luminescence and enhanced photocatalytic activity for Eu(III) doped Bi 2 WO 6 nanoparticles. Spectrochimica Acta - Part A: Molecular and Biomolecular Spectroscopy, 2017, 177, 58-62.	3.9	37
195	Construction of core–shell tecto dendrimers based on supramolecular host–guest assembly for enhanced gene delivery. Journal of Materials Chemistry B, 2017, 5, 8459-8466.	5.8	37
196	Ultrasensitive and selective detection of nicotinamide adenine dinucleotide by target-triggered ligation–rolling circle amplification. Chemical Communications, 2012, 48, 3354.	4.1	36
197	Polymerase/nicking enzyme synergetic isothermal quadratic DNA machine and its application for one-step amplified biosensing of lead (II) ions at femtomole level and DNA methyltransferase. NPG Asia Materials, 2014, 6, e131-e131.	7.9	36
198	Enhanced thermoelectric properties of PEDOT:PSS films via a novel two-step treatment. RSC Advances, 2015, 5, 105592-105599.	3.6	36

#	Article	IF	CITATIONS
199	A novel composite scaffold comprising ultralong hydroxyapatite microtubes and chitosan: preparation and application in drug delivery. Journal of Materials Chemistry B, 2017, 5, 3898-3906.	5.8	36
200	Hydroxyapatite nanowire/collagen elastic porous nanocomposite and its enhanced performance in bone defect repair. RSC Advances, 2018, 8, 26218-26229.	3.6	36
201	Diabetes Exacerbates Myocardial Ischemia/Reperfusion Injury by Down-Regulation of MicroRNA and Up-Regulation of O-GlcNAcylation. JACC Basic To Translational Science, 2018, 3, 350-362.	4.1	36
202	Biocompatibility, Alignment Degree and Mechanical Properties of an Electrospun Chitosan–P(LLA-CL) Fibrous Scaffold. Journal of Biomaterials Science, Polymer Edition, 2009, 20, 2117-2128.	3.5	35
203	Microwave-assisted hydrothermal preparation using adenosine 5â€2-triphosphate disodium salt as a phosphate source and characterization of zinc-doped amorphous calcium phosphate mesoporous microspheres. Microporous and Mesoporous Materials, 2013, 180, 79-85.	4.4	35
204	Preparation of cellulose-graft-polylactic acid via melt copolycondensation for use in polylactic acid based composites: synthesis, characterization and properties. RSC Advances, 2016, 6, 1973-1983.	3.6	35
205	Porous Nanocomposite Comprising Ultralong Hydroxyapatite Nanowires Decorated with Zincâ€Containing Nanoparticles and Chitosan: Synthesis and Application in Bone Defect Repair. Chemistry - A European Journal, 2018, 24, 8809-8821.	3.3	35
206	Calcium Phosphate Hybrid Nanoparticles: Selfâ€Assembly Formation, Characterization, and Application as an Anticancer Drug Nanocarrier. Chemistry - an Asian Journal, 2013, 8, 1306-1312.	3.3	34
207	Synthesis and microphase separated structures of polydimethylsiloxane/polycarbonate-based polyurethanes. RSC Advances, 2013, 3, 8291.	3.6	34
208	Confine Clay in an Alternating Multilayered Structure through Injection Molding: A Simple and Efficient Route to Improve Barrier Performance of Polymeric Materials. ACS Applied Materials & Interfaces, 2015, 7, 10178-10189.	8.0	34
209	99mTc-Labeled RGD–Polyethylenimine Conjugates with Entrapped Gold Nanoparticles in the Cavities for Dual-Mode SPECT/CT Imaging of Hepatic Carcinoma. ACS Applied Materials & Interfaces, 2018, 10, 6146-6154.	8.0	34
210	Converting Immune Cold into Hot by Biosynthetic Functional Vesicles to Boost Systematic Antitumor Immunity. IScience, 2020, 23, 101341.	4.1	34
211	Donut-like MOFs of copper/nicotinic acid and composite hydrogels with superior bioactivity for rh-bFGF delivering and skin wound healing. Journal of Nanobiotechnology, 2021, 19, 275.	9.1	34
212	Interfacial enhancement of maleated polypropylene/silica composites using graphene oxide. Journal of Applied Polymer Science, 2012, 125, E348.	2.6	33
213	BRCAA1 antibody- and Her2 antibody-conjugated amphiphilic polymer engineered CdSe/ZnS quantum dots for targeted imaging of gastric cancer. Nanoscale Research Letters, 2014, 9, 244.	5.7	33
214	Photocatalytic Simultaneous Removal of Nitrite and Ammonia via a Zinc Ferrite/Activated Carbon Hybrid Catalyst under UV–Visible Irradiation. ACS Omega, 2019, 4, 6411-6420.	3.5	33
215	Photothermal-triggered immunogenic nanotherapeutics for optimizing osteosarcoma therapy by synergizing innate and adaptive immunity. Biomaterials, 2022, 282, 121383.	11.4	33
216	Differentiated Visualization of Single-Cell 5-Hydroxymethylpyrimidines with Microfluidic Hydrogel Encoding. Journal of the American Chemical Society, 2020, 142, 2889-2896.	13.7	32

#	Article	IF	CITATIONS
217	High surface area carbonate apatite nanorod bundles: Surfactant-free sonochemical synthesis and drug loading and release properties. Materials Research Bulletin, 2013, 48, 1536-1540.	5.2	31
218	Strong and conductive double-network graphene/PVA gel. RSC Advances, 2014, 4, 39588.	3.6	31
219	Design and analysis of the cross-linked dual helical micromixer for rapid mixing at low Reynolds numbers. Microfluidics and Nanofluidics, 2015, 19, 169-180.	2.2	31
220	Abnormal functional connectivity strength in first-episode, drug-naÃ⁻ve adult patients with major depressive disorder. Progress in Neuro-Psychopharmacology and Biological Psychiatry, 2020, 97, 109759.	4.8	31
221	Extensionâ€induced mechanical reinforcement in meltâ€spun fibers of polyamide 66/multiwalled carbon nanotube composites. Polymer International, 2011, 60, 1646-1654.	3.1	30
222	Nanostructured Calcium Phosphates: Preparation and Their Application in Biomedicine. Nano Biomedicine and Engineering, 2012, 4, .	0.9	30
223	Solvothermal Transformation of a Calcium Oleate Precursor into Largeâ€6ized Highly Ordered Arrays of Ultralong Hydroxyapatite Microtubes. Chemistry - A European Journal, 2014, 20, 7116-7121.	3.3	30
224	Preparation of nylon MXD6/EG/CNTs ternary composites with excellent thermal conductivity and electromagnetic interference shielding effectiveness. Chinese Journal of Polymer Science (English) Tj ETQq0 0 0	rg B3T.\$ Ovei	rlo cto 10 Tf 50
225	3D Multi-Microchannel Helical Mixer Fabricated by Femtosecond Laser inside Fused Silica. Micromachines, 2018, 9, 29.	2.9	30
226	Improving Damping Properties and Thermal Stability of Epoxy/Polyurethane Grafted Copolymer by Adding Glycidyl POSS. Chinese Journal of Polymer Science (English Edition), 2018, 36, 1297-1302.	3.8	30
227	IR Artificial Compound Eye. Advanced Optical Materials, 2020, 8, 1901767.	7.3	30
228	Stabilization of (SnS4)4â^' anion by coordinating to [TM(Ï€-conjugated-ligand)m]n+ complex: a chain-like thiostannate(iv) {[Mn(phen)]2(SnS4)}n·nH2O exhibiting an unprecedented link mode of the (SnS4)4â^' anion. CrystEngComm, 2010, 12, 4035.	2.6	29
229	Preparation, structure and properties of thermoplastic olefin nanocomposites containing functionalized carbon nanotubes. Polymer International, 2011, 60, 1629-1637.	3.1	29
230	Microwave-assisted hydrothermal rapid synthesis of amorphous calcium phosphate nanoparticles and hydroxyapatite microspheres using cytidine 5′-triphosphate disodium salt as a phosphate source. Materials Letters, 2014, 124, 208-211.	2.6	29
231	Templated solvothermal synthesis of magnesium silicate hollow nanospheres with ultrahigh specific surface area and their application in high-performance protein adsorption and drug delivery. Journal of Materials Chemistry B, 2016, 4, 3257-3268.	5.8	29
232	Great Framework Variation of Polymers in the Manganese(II) Maleate/α,α′-Diimine System: Syntheses, Structures, and Magneto-Structural Correlation. European Journal of Inorganic Chemistry, 2003, 2003, 2872-2879.	2.0	28
233	Inhibitory Impact of 3′-Terminal 2′-O-Methylated Small Silencing RNA on Target-Primed Polymerization and Unbiased Amplified Quantification of the RNA in <i>Arabidopsis thaliana</i> . Analytical Chemistry, 2015, 87, 8758-8764.	6.5	28
234	Integration of Great Water Repellence and Imaging Performance on a Superhydrophobic PDMS Microlens Array by Femtosecond Laser Microfabrication. Advanced Engineering Materials, 2019, 21, 1800994.	3.5	28

#	Article	IF	CITATIONS
235	Effect of molecular weight on the properties of poly(butylene succinate). Chinese Journal of Polymer Science (English Edition), 2014, 32, 953-960.	3.8	27
236	Yolkâ€Shell Porous Microspheres of Calcium Phosphate Prepared by Using Calcium <scp>L</scp> ‣actate and Adenosine 5′â€Triphosphate Disodium Salt: Application in Protein/Drug Delivery. Chemistry - A European Journal, 2015, 21, 9868-9876.	3.3	27
237	Microwave-assisted solvothermal synthesis and upconversion luminescence of CaF2:Yb3+/Er3+ nanocrystals. Journal of Colloid and Interface Science, 2015, 440, 39-45.	9.4	27
238	DNA-templated microwave-hydrothermal synthesis of nanostructured hydroxyapatite for storing and sustained release of an antibacterial protein. Dalton Transactions, 2016, 45, 1648-1656.	3.3	27
239	Engineered Janus probes modulate nucleic acid amplification to expand the dynamic range for direct detection of viral genomes in one microliter crude serum samples. Chemical Science, 2018, 9, 392-397.	7.4	27
240	Super Strong All-Cellulose Composite Filaments by Combination of Inducing Nanofiber Formation and Adding Nanofibrillated Cellulose. Biomacromolecules, 2018, 19, 4386-4395.	5.4	27
241	The hydroxyapatite microtubes enhanced GelMA hydrogel scaffold with inner "pipeline framework― structure for bone tissue regeneration. Composites Part B: Engineering, 2022, 228, 109396.	12.0	27
242	Single-step rapid microwave-assisted synthesis of polyacrylamide–calcium phosphate nanocomposites in aqueous solution. Materials Letters, 2009, 63, 1332-1334.	2.6	26
243	Two-Dimensional Porous SiO ₂ Nanostructures Derived from Renewable Petal Cells with Enhanced Adsorption Efficiency for Removal of Hazardous Dye. ACS Sustainable Chemistry and Engineering, 2017, 5, 3478-3487.	6.7	26
244	Ultralong hydroxyapatite nanowires/collagen scaffolds with hierarchical porous structure, enhanced mechanical properties and excellent cellular attachment. Ceramics International, 2017, 43, 15747-15754.	4.8	26
245	Selenium-doped hydroxyapatite biopapers with an anti-bone tumor effect by inducing apoptosis. Biomaterials Science, 2019, 7, 5044-5053.	5.4	26
246	Simple fabrication of closed-packed IR microlens arrays on silicon by femtosecond laser wet etching. Applied Physics A: Materials Science and Processing, 2015, 121, 157-162.	2.3	25
247	Durability of the tunable adhesive superhydrophobic PTFE surfaces for harsh environment applications. Applied Physics A: Materials Science and Processing, 2016, 122, 1.	2.3	25
248	Strengthening and toughening of thermoplastic polyolefin elastomer using polypropyleneâ€grafted multiwalled carbon nanotubes. Journal of Applied Polymer Science, 2011, 121, 2104-2112.	2.6	24
249	Electrospinning of calcium phosphate-poly(D,L-lactic acid) nanofibers for sustained release of water-soluble drug and fast mineralization. International Journal of Nanomedicine, 2016, Volume 11, 5087-5097.	6.7	24
250	Dopamine-modified highly porous hydroxyapatite microtube networks with efficient near-infrared photothermal effect, enhanced protein adsorption and mineralization performance. Colloids and Surfaces B: Biointerfaces, 2017, 159, 337-348.	5.0	24
251	Remote, selective, and in situ manipulation of liquid droplets on a femtosecond laser-structured superhydrophobic shape-memory polymer by near-infrared light. Science China Chemistry, 2021, 64, 861-872.	8.2	24
252	A Universal Mechanochemistry Allows Onâ€Demand Synthesis of Stable and Processable Liquid Metal Composites. Small Methods, 2022, 6, .	8.6	24

#	Article	IF	CITATIONS
25	The effects of antidepressant treatment on serotonergic and dopaminergic systems in Fawn–Hooded rats: a quantitative autoradiography study. Brain Research, 2003, 976, 22-29.	2.2	23
25	Calcium Phosphate Nanocarriers Dual‣oaded with Bovine Serum Albumin and Ibuprofen: Facile 4 Synthesis, Sequential Drug Loading and Sustained Drug Release. Chemistry - an Asian Journal, 2012, 7, 1610-1615.	3.3	23
25	Core–Shell Hollow Microspheres of Magnetic Iron Oxide@Amorphous Calcium Phosphate: Synthesis Using Adenosine 5â€2â€Triphosphate and Application in pHâ€Responsive Drug Delivery. Chemistry - an Asian Journal, 2014, 9, 2908-2914.	3.3	23
25	Multifunctional biodegradable terbium-doped calcium phosphate nanoparticles: facile preparation, pH-sensitive drug release and in vitro bioimaging. RSC Advances, 2014, 4, 53122-53129.	3.6	23
25	Microwaveâ€Assisted Hydrothermal Rapid Synthesis of Amorphous Calcium Phosphate Mesoporous Microspheres Using Adenosine 5â€2â€Diphosphate and Application in pHâ€Responsive Drug Delivery. Chemist - an Asian Journal, 2015, 10, 2503-2511.	try 3.3	23
25	Amorphous calcium phosphate nanowires prepared using beta-glycerophosphate disodium salt as an organic phosphate source by a microwave-assisted hydrothermal method and adsorption of heavy metals in water treatment. RSC Advances, 2015, 5, 40154-40162.	3.6	23
25	Fabrication of electrospun PVDF nanofibers with higher content of polar β phase and smaller diameter 9 by adding a small amount of dioctadecyl dimethyl ammonium chloride. Chinese Journal of Polymer Science (English Edition), 2017, 35, 992-1000.	3.8	23
26	O Ultralong hydroxyapatite microtubes: solvothermal synthesis and application in drug loading and sustained drug release. CrystEngComm, 2017, 19, 1965-1973.	2.6	23
26	underwater Transparent Miniature "Mechanical Hand―Based on Femtosecond Laser-Induced Controllable Oil-Adhesive Patterned Glass for Oil Droplet Manipulation. Langmuir, 2017, 33, 3659-3665.	3.5	23
26	All-in-One Synchronized DNA Nanodevices Facilitating Multiplexed Cell Imaging. Analytical Chemistry, 2019, 91, 4696-4701.	6.5	23
26	Tannic Acid: A green and efficient stabilizer of Au, Ag, Cu and Pd nanoparticles for the 4-Nitrophenol Reduction, Suzuki–Miyaura coupling reactions and click reactions in aqueous solution. Journal of Colloid and Interface Science, 2021, 604, 281-291.	9.4	23
26	Solvothermal synthesis, characterization and magnetic properties of α-Fe2O3 and Fe3O4 flower-like hollow microspheres. Journal of Solid State Chemistry, 2013, 199, 204-211.	2.9	22
26	Amorphous magnesium phosphate flower-like hierarchical nanostructures: microwave-assisted rapid synthesis using fructose 1,6-bisphosphate trisodium salt as an organic phosphorus source and application in protein adsorption. RSC Advances, 2015, 5, 14906-14915.	3.6	22
26	MtDNA analysis reveals enriched pathogenic mutations in Tibetan highlanders. Scientific Reports, 2016, 6, 31083.	3.3	22
26	A facile way to large-scale production of few-layered graphene via planetary ball mill. Chinese Journal of Polymer Science (English Edition), 2016, 34, 1270-1280.	3.8	22
26	Femtosecond-Laser-Produced Underwater "Superpolymphobic―Nanorippled Surfaces: Repelling Liquid 8 Polymers in Water for Applications of Controlling Polymer Shape and Adhesion. ACS Applied Nano Materials, 2019, 2, 7362-7371.	5.0	22
26	9 Femtosecond Laser-Induced Underwater Superoleophobic Surfaces with Reversible pH-Responsive Wettability. Langmuir, 2019, 35, 3295-3301.	3.5	22
27	Magnetically Controllable Isotropic/Anisotropic Slippery Surface for Flexible Droplet Manipulation. Langmuir, 2020, 36, 15403-15409.	3.5	22

#	Article	IF	CITATIONS
271	Underwater Superaerophobicity/Superaerophilicity and Unidirectional Bubble Passage Based on the Femtosecond Laserâ€Structured Stainless Steel Mesh. Advanced Materials Interfaces, 2020, 7, 1902128.	3.7	22
272	Calcium phosphate/block copolymer hybrid porous nanospheres: Preparation and application in drug delivery. Materials Letters, 2010, 64, 2299-2301.	2.6	21
273	High-Performance Laser Beam Homogenizer Based on Double-Sided Concave Microlens. IEEE Photonics Technology Letters, 2014, 26, 2086-2089.	2.5	21
274	Synthesis, characterization and applications of calcium carbonate/fructose 1,6-bisphosphate composite nanospheres and carbonated hydroxyapatite porous nanospheres. Journal of Materials Chemistry B, 2014, 2, 8378-8389.	5.8	21
275	Hydrothermal synthesis of hydroxyapatite nanorods using pyridoxal-5′-phosphate as a phosphorus source. Materials Research Bulletin, 2014, 55, 67-70.	5.2	21
276	Diagnostic Accuracy of Noncontrast CT in Detecting Acute Appendicitis: A Meta-analysis of Prospective Studies. American Surgeon, 2015, 81, 626-629.	0.8	21
277	Femtosecond laser controlling underwater oil-adhesion of glass surface. Applied Physics A: Materials Science and Processing, 2015, 119, 837-844.	2.3	21
278	Magnesium whitlockite hollow microspheres: a comparison of microwave-hydrothermal and conventional hydrothermal syntheses using fructose 1,6-bisphosphate, and application in protein adsorption. RSC Advances, 2016, 6, 33393-33402.	3.6	21
279	Enzymatic Reaction Generates Biomimic Nanominerals with Superior Bioactivity. Small, 2018, 14, e1804321.	10.0	21
280	Microfluidic Channels Fabrication Based on Underwater Superpolymphobic Microgrooves Produced by Femtosecond Laser Direct Writing. ACS Applied Polymer Materials, 2019, 1, 2819-2825.	4.4	21
281	Femtosecond Laser-Structured Underwater "Superpolymphobic―Surfaces. Langmuir, 2019, 35, 9318-9322.	3.5	21
282	Microwave-assisted rapid synthesis of magnesium phosphate hydrate nanosheets and their application in drug delivery and protein adsorption. Journal of Materials Chemistry B, 2014, 2, 8576-8586.	5.8	20
283	Effect of chain structure on the thermal conductivity of expanded graphite/polymer composites. RSC Advances, 2016, 6, 10185-10191.	3.6	20
284	Magnesium phosphate pentahydrate nanosheets: Microwave-hydrothermal rapid synthesis using creatine phosphate as an organic phosphorus source and application in protein adsorption. Journal of Colloid and Interface Science, 2016, 462, 297-306.	9.4	20
285	Green and Economical Strategy for Spinning Robust Cellulose Filaments. ACS Sustainable Chemistry and Engineering, 2020, 8, 14927-14937.	6.7	20
286	Enhanced interfacial adhesion via interfacial crystallization between sisal fiber and isotactic polypropylene: direct evidence from single-fiber fragmentation testing. Polymer International, 2014, 63, 646-651.	3.1	19
287	The effect of hard block content on the orientation and mechanical properties of olefin block copolymer films as obtained <i>via</i> melt stretching. RSC Advances, 2015, 5, 82535-82543.	3.6	19
288	Functional and Biomimetic DNA Nanostructures on Lipid Membranes. Langmuir, 2018, 34, 14721-14730.	3.5	19

#	Article	IF	CITATIONS
289	A high-efficiency three-dimensional helical micromixer in fused silica. Microsystem Technologies, 2013, 19, 1033-1040.	2.0	18
290	Process for the fabrication of complex three-dimensional microcoils in fused silica. Optics Letters, 2013, 38, 2911.	3.3	18
291	Largely Improved Mechanical Properties of a Poly(styrene- <i>b</i> -isoprene- <i>b</i> -styrene) Thermoplastic Elastomer Prepared under Dynamic-Packing Injection Molding. Industrial & Engineering Chemistry Research, 2014, 53, 15287-15295.	3.7	18
292	Using an "underwater superoleophobic pattern―to make a liquid lens array. RSC Advances, 2015, 5, 40907-40911.	3.6	18
293	A femtosecond laser-induced superhygrophobic surface: beyond superhydrophobicity and repelling various complex liquids. RSC Advances, 2019, 9, 6650-6657.	3.6	18
294	Reducing Adhesion for Dispensing Tiny Water/Oil Droplets and Gas Bubbles by Femtosecond Laserâ€Treated Needle Nozzles: Superhydrophobicity, Superoleophobicity, and Superaerophobicity. ChemNanoMat, 2019, 5, 241-249.	2.8	18
295	Facile Construction of Porous Magnetic Nanoparticles from Ferrocene-Functionalized Polyhedral Oligomeric Silsesquioxane-Containing Microparticles for Dye Adsorption. Industrial & Engineering Chemistry Research, 2020, 59, 9532-9540.	3.7	18
296	Aptamer-Functionalized Microdevices for Bioanalysis. ACS Applied Materials & Interfaces, 2021, 13, 9402-9411.	8.0	18
297	Liquidâ€Infused Slippery Stainless Steel Surface Prepared by Alcoholâ€Assisted Femtosecond Laser Ablation. Advanced Materials Interfaces, 2021, 8, 2001334.	3.7	18
298	Photoredox-Catalyzed Addition of Dibromofluoromethane to Alkenes: Direct Synthesis of 1-Bromo-1-fluoroalkanes. Organic Letters, 2021, 23, 2364-2369.	4.6	18
299	Preparation of expanded graphite/poly (phenylene sulfide) composites with high thermal and electrical conductivity by rotating solid-state premixing and melt processing. Journal of Materials Science, 2013, 48, 1932-1939.	3.7	17
300	Preparation of Polylactide Composite with Excellent Flame Retardance and Improved Mechanical Properties. Chinese Journal of Polymer Science (English Edition), 2018, 36, 1385-1393.	3.8	17
301	Intracellular Entropyâ€Driven Multiâ€Bit DNA Computing for Tumor Progression Discrimination. Angewandte Chemie, 2020, 132, 13369-13374.	2.0	17
302	Simple and Low-Cost Oil/Water Separation Based on the Underwater Superoleophobicity of the Existing Materials in Our Life or Nature. Frontiers in Chemistry, 2020, 8, 507.	3.6	17
303	Cellular macromolecules-tethered DNA walking indexing to explore nanoenvironments of chromatin modifications. Nature Communications, 2021, 12, 1965.	12.8	17
304	Simultaneous improvements of thermal stability and mechanical properties of poly(propylene) Tj ETQq0 0 0 rgB Science (English Edition), 2014, 32, 1724-1736.	T /Overloc 3.8	k 10 Tf 50 14 16
305	Effect of melting temperature on interfacial interaction and mechanical properties of polypropylene (PP) fiber reinforced olefin block copolymers (OBCs). RSC Advances, 2014, 4, 45234-45243.	3.6	16
306	Using POSS–C ₆₀ giant molecules as a novel compatibilizer for PS/PMMA polymer blends. RSC Advances, 2016, 6, 18924-18928	3.6	16

#	Article	IF	CITATIONS
307	DNAâ€Mediated Assembly of Gold Nanoparticles and Applications in Bioanalysis. ChemNanoMat, 2017, 3, 725-735.	2.8	16
308	Trapped Airâ€Induced Reversible Transition between Underwater Superaerophilicity and Superaerophobicity on the Femtosecond Laserâ€Ablated Superhydrophobic PTFE Surfaces. Advanced Materials Interfaces, 2019, 6, 1900262.	3.7	16
309	Enhanced thermal conductivity and wear resistance of polytetrafluoroethylene via incorporating hexagonal boron nitride and alumina particles. Journal of Applied Polymer Science, 2022, 139, 51497.	2.6	16
310	Water/gas separation based on the selective bubble-passage effect of underwater superaerophobic and superaerophilic meshes processed by a femtosecond laser. Nanoscale, 2021, 13, 10414-10424.	5.6	16
311	Maternal high estradiol exposure alters CDKN1C and IGF2 expression in human placenta. Placenta, 2018, 61, 72-79.	1.5	16
312	Computer-aided design of reversible hybridization chain reaction (CAD-HCR) enables multiplexed single-cell spatial proteomics imaging. Science Advances, 2022, 8, eabk0133.	10.3	16
313	Autoradiographic quantification of neurochemical markers of serotonin, dopamine and opioid systems in rat brain mesolimbic regions following chronic St. John's wort treatment. Naunyn-Schmiedeberg's Archives of Pharmacology, 2003, 367, 126-133.	3.0	15
314	Sequence-length variation of mtDNA HVS-I C-stretch in Chinese ethnic groups. Journal of Zhejiang University: Science B, 2009, 10, 711-720.	2.8	15
315	Effect of melt temperature on the phase morphology, thermal behavior and mechanical properties of injection-molded PP/LLDPE blends. Chinese Journal of Polymer Science (English Edition), 2010, 28, 249-255.	3.8	15
316	Shape measurement of objects using an ultrafast optical Kerr gate of bismuth glass. Journal of Applied Physics, 2010, 107, 043104.	2.5	15
317	Synergistic effects of βâ€modification and impact polypropylene copolymer on brittleâ€ductile transition of polypropylene random copolymer. Journal of Applied Polymer Science, 2013, 129, 3613-3622.	2.6	15
318	Hydrothermal synthesis of nanorod-assembled porous microspheres of hydroxyapatite/casein using ATP as a phosphorus source and casein sodium salt as a template. Materials Letters, 2015, 160, 242-245.	2.6	15
319	The effect of DBP of carbon black on the dynamic self-assembly in a polymer melt. RSC Advances, 2016, 6, 24843-24852.	3.6	15
320	Reversible switch between underwater superaerophilicity and superaerophobicity on the superhydrophobic nanowire-haired mesh for controlling underwater bubble wettability. AIP Advances, 2018, 8, .	1.3	15
321	Underwater Anisotropic 3D Superoleophobic Tracks Applied for the Directional Movement of Oil Droplets and the Microdroplets Reaction. Advanced Materials Interfaces, 2019, 6, 1900067.	3.7	15
322	Liquid Metal-Based Reconfigurable and Repairable Electronics Designed by a Femtosecond Laser. ACS Applied Electronic Materials, 2020, 2, 2685-2691.	4.3	15
323	Filtration and removal of liquid polymers from water (polymer/water separation) by use of the underwater superpolymphobic mesh produced with a femtosecond laser. Journal of Colloid and Interface Science, 2021, 582, 1203-1212.	9.4	15
324	Pairwise Proximityâ€Differentiated Visualization of Singleâ€Cell DNA Epigenetic Marks. Angewandte Chemie - International Edition, 2021, 60, 3428-3432.	13.8	15

#	Article	IF	CITATIONS
325	Intrauterine hyperglycemia induces intergenerational Dlk1-Gtl2 methylation changes in mouse placenta. Oncotarget, 2018, 9, 22398-22405.	1.8	15
326	Hydrothermal synthesis of relatively uniform CePO4@LaPO4 one-dimensional nanostructures with highly improved luminescence. Journal of Alloys and Compounds, 2010, 492, 559-563.	5.5	14
327	High speed injection molding of high density polyethylene — Effects of injection speed on structure and properties. Chinese Journal of Polymer Science (English Edition), 2011, 29, 456-464.	3.8	14
328	Time-resolved single-shot imaging of femtosecond laser induced filaments using supercontinuum and optical polarigraphy. Applied Physics Letters, 2012, 100, .	3.3	14
329	The interfacial enhancement of LLDPE/whisker composites via interfacial crystallization. Polymers for Advanced Technologies, 2012, 23, 431-440.	3.2	14
330	A Simple Way to Fabricate Close-Packed High Numerical Aperture Microlens Arrays. IEEE Photonics Technology Letters, 2013, 25, 1336-1339.	2.5	14
331	Microwave-Assisted Hydrothermal Rapid Synthesis of Calcium Phosphates: Structural Control and Application in Protein Adsorption. Nanomaterials, 2015, 5, 1284-1296.	4.1	14
332	Trifunctional molecular beacon-mediated quadratic amplification for highly sensitive and rapid detection of mercury(II) ion with tunable dynamic range. Biosensors and Bioelectronics, 2016, 86, 892-898.	10.1	14
333	Tunable potential well for plasmonic trapping of metallic particles by bowtie nano-apertures. Scientific Reports, 2016, 6, 32675.	3.3	14
334	Zeroâ€Background Helicaseâ€Dependent Amplification and Its Application to Reliable Assay of Telomerase Activity in Cancer Cell by Eliminating Primer–Dimer Artifacts. ChemBioChem, 2016, 17, 1171-1176.	2.6	14
335	Fabrication of Chalcogenide Glass Based Hexagonal Gapless Microlens Arrays via Combining Femtosecond Laser Assist Chemical Etching and Precision Glass Molding Processes. Materials, 2020, 13, 3490.	2.9	14
336	Bioinspired Artificial Compound Eyes: Characteristic, Fabrication, and Application. Advanced Materials Technologies, 2021, 6, 2100091.	5.8	14
337	Sunlight Recovering the Superhydrophobicity of a Femtosecond Laser-Structured Shape-Memory Polymer. Langmuir, 2022, 38, 4645-4656.	3.5	14
338	High-aspect-ratio grooves fabricated in silicon by a single pass of femtosecond laser pulses. Journal of Applied Physics, 2012, 111, 093102.	2.5	13
339	Combined effect of βâ€nucleating agent and processing melt temperature on the toughness of impact polypropylene copolymer. Polymer International, 2013, 62, 172-178.	3.1	13
340	Cascaded optical limiter with low activating and high damage thresholds using single-layer graphene and single-walled carbon nanotubes. Journal of Applied Physics, 2014, 115, .	2.5	13
341	Superparamagnetic yolk–shell porous nanospheres of iron oxide@magnesium silicate: synthesis and application in high-performance anticancer drug delivery. RSC Advances, 2016, 6, 103399-103411.	3.6	13
342	Association between premature ovarian failure, polymorphisms in MTHFR and MTRR genes and serum homocysteine concentration. Reproductive BioMedicine Online, 2016, 32, 407-413.	2.4	13

#	Article	IF	CITATIONS
343	A widely applicable method to fabricate underwater superoleophobic surfaces with low oil-adhesion on different metals by a femtosecond laser. Applied Physics A: Materials Science and Processing, 2017, 123, 1.	2.3	13
344	Click-encoded rolling FISH for visualizing single-cell RNA polyadenylation and structures. Nucleic Acids Research, 2019, 47, e145-e145.	14.5	13
345	Preparation and Properties of Ultrathin Flexible Expanded Graphite Film via Adding Natural Rubber. Chinese Journal of Polymer Science (English Edition), 2019, 37, 806-814.	3.8	13
346	Adsorbability of Modified PBS Nanofiber Membrane to Heavy Metal Ions and Dyes. Journal of Polymers and the Environment, 2021, 29, 3029-3039.	5.0	13
347	Near-infrared light excited UCNP-DNAzyme nanosensor for selective detection of Pb2+ and in vivo imaging. Talanta, 2021, 227, 122156.	5.5	13
348	Nanosized BaSnO ₃ as Electron Transport Promoter Coupled with gâ€C ₃ N ₄ toward Enhanced Photocatalytic H ₂ Production. Advanced Sustainable Systems, 2021, 5, 2100138.	5.3	13
349	Simple Enzyme-Free Biosensor for Highly Sensitive and Selective Detection of miR-21 Based on Multiple Signal Amplification Strategy. Journal of Analysis and Testing, 2022, 6, 36-43.	5.1	13
350	Largely improved tensile extensibility of poly(<scp>L</scp> â€lactic acid) by adding poly(εâ€caprolactone). Polymer International, 2010, 59, 1154-1161.	3.1	12
351	Preparation and properties of poly(ethylene terephthalate)/inorganic whiskers composites. Journal of Applied Polymer Science, 2011, 121, 604-611.	2.6	12
352	Microwave-assisted rapid synthesis of magnesium phosphate hierarchical structures using adenosine 5′-triphosphate disodium salt as a phosphorus source. Materials Letters, 2015, 140, 79-82.	2.6	12
353	Sonochemical synthesis of fructose 1,6-bisphosphate dicalcium porous microspheres and their application in promotion of osteogenic differentiation. Materials Science and Engineering C, 2017, 77, 846-856.	7.3	12
354	Knockdown of PEBP4 inhibits human glioma cell growth and invasive potential via ERK1/2 signaling pathway. Molecular Carcinogenesis, 2019, 58, 135-143.	2.7	12
355	Emerging Separation Applications of Surface Superwettability. Nanomaterials, 2022, 12, 688.	4.1	12
356	Ti3C2Tx MXene-Coated Electrospun PCL Conduits for Enhancing Neurite Regeneration and Angiogenesis. Frontiers in Bioengineering and Biotechnology, 2022, 10, 850650.	4.1	12
357	Tailoring toughness of injection molded bar of polypropylene random copolymer through processing melt temperature. Polymer International, 2011, 60, 1705-1714.	3.1	11
358	Effect of surface wettability on transparency in different water conditions. Journal of Coatings Technology Research, 2013, 10, 641-647.	2.5	11
359	Simply controllable growth of single crystal plasmonic Au–Ag nano-spines with anisotropic multiple sites for highly sensitive and uniform surface-enhanced Raman scattering sensing. RSC Advances, 2016, 6, 66056-66065.	3.6	11
360	Excellent Surface Enhanced Raman Scattering of SiO2 Fiber Membrane Embedded with Ag Nanoparticles. Journal of Inorganic and Organometallic Polymers and Materials, 2018, 28, 251-257.	3.7	11

#	Article	IF	CITATIONS
361	Synergistic enhancement in tensile strength and ductility of ABS by using recycled PETG plastic. Journal of Applied Polymer Science, 2009, 113, 1207-1215.	2.6	10
362	Fabrication of quasi-periodic micro-voids in fused silica byÂsingleÂfemtosecond laser pulse. Applied Physics A: Materials Science and Processing, 2011, 102, 39-44.	2.3	10
363	Ordered longâ€helical conformation of isotactic polypropylene obtained in constrained environment of nanoclay. Polymers for Advanced Technologies, 2011, 22, 1375-1380.	3.2	10
364	Morphology and mechanical properties of poly(ethyleneoctene) copolymers obtained by dynamic packing injection molding. Chinese Journal of Polymer Science (English Edition), 2012, 30, 603-612.	3.8	10
365	The effect of silica morphology on properties of PVA/silica nano-composites. Chinese Journal of Polymer Science (English Edition), 2013, 31, 1546-1553.	3.8	10
366	Porous Microspheres of Casein/Amorphous Calcium Phosphate Nanocomposite: Room Temperature Synthesis and Application in Drug Delivery. Current Nanoscience, 2015, 12, 70-78.	1.2	10
367	A novel biodegradable phosphorus-containing copolyester with preferable flame retardancy and mechanical properties. RSC Advances, 2015, 5, 61364-61370.	3.6	10
368	An amorphous calcium phosphate nanocomposite for storing and sustained release of IgY protein with antibacterial activity. RSC Advances, 2015, 5, 100682-100688.	3.6	10
369	Property enhancement of graphene fiber by adding small loading of cellulose nanofiber. Nanocomposites, 2016, 2, 8-17.	4.2	10
370	Antibacterial gluey silver–calcium phosphate composites for dentine remineralization. Journal of Materials Chemistry B, 2018, 6, 4985-4994.	5.8	10
371	Mini-Review on Bioinspired Superwetting Microlens Array and Compound Eye. Frontiers in Chemistry, 2020, 8, 575786.	3.6	10
372	Fabrication of ZnSe Microlens Array for a Wide Infrared Spectral Region. IEEE Photonics Technology Letters, 2020, 32, 1327-1330.	2.5	10
373	Tuning a surface super-repellent to liquid metal by a femtosecond laser. RSC Advances, 2020, 10, 3301-3306.	3.6	10
374	Superwettabilityâ€based separation: From oil/water separation to polymer/water separation and bubble/water separation. Nano Select, 2021, 2, 1580-1588.	3.7	10
375	Everolimus halts hepatic cystogenesis in a rodent model of polycystic-liver-disease. World Journal of Gastroenterology, 2017, 23, 5499.	3.3	10
376	Slippery Liquidâ€Infused Porous Surface on Metal Material with Excellent Ice Resistance Fabricated by Femtosecond Bessel Laser. Advanced Engineering Materials, 2022, 24, .	3.5	10
377	<i>para</i> -Aramid Nanofiber Membranes for High-Performance and Multifunctional Materials. ACS Applied Nano Materials, 2022, 5, 747-758.	5.0	10
378	Epitaxial crystallization and oriented structure of linear lowâ€density polyethylene/isotactic polypropylene blends obtained via dynamic packing injection molding. Polymers for Advanced Technologies, 2011, 22, 225-231.	3.2	9

FENG CHEN

#	Article	IF	CITATIONS
379	A simple method for fabrication of high-aspect-ratio all-silicon grooves. Applied Surface Science, 2013, 284, 372-378.	6.1	9

Toughening of polycarbonate through reactive melt blending: Effect of hydroxyl content and viscosity of hydroxyl-terminated polydimethysiloxane. Chinese Journal of Polymer Science (English) Tj ETQq0 0 0 rgBIs/Overlogk 10 Tf 50 380

381	Highly porous ceramics based on ultralong hydroxyapatite nanowires. RSC Advances, 2016, 6, 102003-102009.	3.6	9
382	Largely enhanced electrical properties of polymer composites via the combined effect of volume exclusion and synergy. RSC Advances, 2016, 6, 51900-51907.	3.6	9
383	Catalase-functionalized SiO ₂ nanoparticles mediate growth of gold nanoparticles for plasmonic biosensing of attomolar microRNA with the naked eye. RSC Advances, 2016, 6, 15709-15715.	3.6	9
384	Ultraviolet light-induced photochemical reaction for controlled fabrication of Ag nano-islands on ZnO nanosheets: an advanced inexpensive substrate for ultrasensitive surface-enhanced Raman scattering analysis. Optical Materials Express, 2017, 7, 3137.	3.0	9
385	Ordinary Optical Fiber Sensor for Ultra-High Temperature Measurement Based on Infrared Radiation. Sensors, 2018, 18, 4071.	3.8	9
386	Preparation of porous calcium phosphate microspheres with phosphate-containing molecules at room temperature for drug delivery and osteogenic differentiation. RSC Advances, 2018, 8, 25480-25488.	3.6	9
387	Spherical hybrid filler <scp>BN</scp> @ <scp>Al₂O₃</scp> via chemical adhesive for enhancing thermal conductivity and processability of silicon rubber. Journal of Applied Polymer Science, 2021, 138, 51211.	2.6	9
388	Amorphous calcium magnesium phosphate nanocomposites with superior osteogenic activity for bone regeneration. International Journal of Energy Production and Management, 2021, 8, rbab068.	3.7	9
389	Biomineralization-inspired synthesis of amorphous manganese phosphates for GLUT5-targeted drug-free catalytic therapy of osteosarcoma. Nanoscale, 2022, 14, 898-909.	5.6	9
390	A facile preparation route for netlike microstructures on a stainless steel using an ethanol-mediated femtosecond laser irradiation. Materials Science and Engineering C, 2013, 33, 663-667.	7.3	8
391	Towards high molecular weight poly(bisphenol a carbonate) with excellent thermal stability and mechanical properties by solid-state polymerization. Chinese Journal of Polymer Science (English) Tj ETQq1 1 0.7	784 3.8 4 rgl	BT \$ Overloc
392	Facile Synthesis of Co3O4 Nanoparticle-Functionalized Mesoporous SiO2 for Catalytic Degradation of Methylene Blue from Aqueous Solutions. Catalysts, 2019, 9, 809.	3.5	8
393	Visualizing Newly Synthesized RNA by Bioorthogonal Labeling-Primed DNA Amplification. Analytical Chemistry, 2020, 92, 8444-8449.	6.5	8
394	The mineralization, drug release and <i>in vivo</i> bone defect repair properties of calcium phosphates/PLA modified tantalum scaffolds. RSC Advances, 2020, 10, 7708-7717.	3.6	8
395	Simultaneous Tuning Band Gaps of Cu ₂ O and TiO ₂ to Form S‣cheme Heteroâ€Photocatalyst. Chemistry - A European Journal, 2021, 27, 14638-14644.	3.3	8
396	Investigation of the intermediates formed during the degradation of Malachite Green in the presence of Fe3+ and H2O2 under visible irradiation. Research on Chemical Intermediates, 2001, 27, 237-248.	2.7	7

#	Article	IF	CITATIONS
397	Stretch-Induced Shish-Kebabs in Rubbery Poly(L-Lactide). Journal of Macromolecular Science - Physics, 2011, 50, 2042-2049.	1.0	7
398	Synthesis and characterization of the tellurium/calcium silicate nanocomposite. Materials Letters, 2011, 65, 424-426.	2.6	7
399	Ultrafast dynamics of thermionic emission on Au film under femtosecond laser excitation. Applied Physics A: Materials Science and Processing, 2013, 112, 479-483.	2.3	7
400	Chirp structure measurement of a supercontinuum pulse based on transient lens effect in tellurite glass. Journal of Applied Physics, 2013, 113, 113106.	2.5	7
401	Novel interconnected nanochannel hydroxyapatite ceramics: synthesis, microstructure, and permeability. Ceramics International, 2017, 43, 5403-5411.	4.8	7
402	Electrospinning synthesis of N-doped TiO2 fiber membranes and its enhanced photocatalysis performance. Chemical Papers, 2021, 75, 115-122.	2.2	7
403	Simultaneous Measurement of Temperature and Refractive Index Using High Temperature Resistant Pure Quartz Grating Based on Femtosecond Laser and HF Etching. Materials, 2021, 14, 1028.	2.9	7
404	Development and Clinical Translation of a Perioperative Nomogram Incorporating Free Fatty Acids to Predict Poor Outcome of Aneurysmal Subarachnoid Hemorrhage Following Endovascular Treatment. Frontiers in Neurology, 2021, 12, 629997.	2.4	7
405	Fabrication of a Chalcogenide Glass Microlens Array for Infrared Laser Beam Homogenization. Materials, 2021, 14, 5952.	2.9	7
406	Polarization Dependence of Femtosecond Optical Kerr Signals in Bismuth Glasses. IEEE Photonics Technology Letters, 2009, 21, 1606-1608.	2.5	6
407	Interfacial enhancement of poly(ethylene terephthalate)/silica composites using graphene oxide. Journal of Materials Research, 2012, 27, 2360-2367.	2.6	6
408	Multi-Frame Observation of a Single Femtosecond Laser Pulse Propagation Using an Echelon and Optical Polarigraphy Technique. IEEE Photonics Technology Letters, 2013, 25, 1879-1881.	2.5	6
409	C5b-9-Targeted Molecular MR Imaging in Rats with Heymann Nephritis: A New Approach in the Evaluation of Nephrotic Syndrome. PLoS ONE, 2015, 10, e0121244.	2.5	6
410	A new understanding concerning the influence of structural changes on the thermal behavior of cellulose. Journal of Polymer Research, 2015, 22, 1.	2.4	6
411	Analysis of Asymmetric Dipoles Interacting in Heterogeneous Metal Nanorod Dimers. Plasmonics, 2015, 10, 1325-1330.	3.4	6
412	RNA-Primed Amplification for Noise-Suppressed Visualization of Single-Cell Splice Variants. Analytical Chemistry, 2020, 92, 9356-9361.	6.5	6
413	Selenium-doped calcium phosphate biomineral reverses multidrug resistance to enhance bone tumor chemotherapy. Nanomedicine: Nanotechnology, Biology, and Medicine, 2021, 32, 102322.	3.3	6
414	Rapid Fabrication of Large-Area Concave Microlens Array on ZnSe. Micromachines, 2021, 12, 458.	2.9	6

#	Article	IF	CITATIONS
415	Phosphorylation of transâ€active response DNAâ€binding proteinâ€of 43ÂkDa promotes its cytoplasmic aggregation and modulates its function in tau mRNA stability and exon 10 alternative splicing. Journal of Neurochemistry, 2021, 158, 766-778.	3.9	6
416	Shearâ€induced clay dispersion in HDPE/PEgMA/organoclay composites as studied via realâ€time rheological method. Journal of Polymer Science, Part B: Polymer Physics, 2010, 48, 302-312.	2.1	5
417	Elimination of the coherent effect in the optical Kerr measurement of bismuth glass using supercontinuum. Journal of Applied Physics, 2011, 109, 123104.	2.5	5
418	Effect of microdomain structure on the mechanical behavior of binary blends. Chinese Journal of Polymer Science (English Edition), 2015, 33, 964-975.	3.8	5
419	Research on hot embossing process of high fill factor microlens array. Microsystem Technologies, 2015, 21, 2109-2114.	2.0	5
420	Preparation of poly(p-phenylene sulfide)/carbon composites with enhanced thermal conductivity and electrical insulativity via hybrids of boron nitride and carbon fillers. Journal Wuhan University of Technology, Materials Science Edition, 2015, 30, 562-567.	1.0	5
421	Localized surface plasmon resonances in core-embedded heterogeneous nano-bowtie antenna. Applied Physics B: Lasers and Optics, 2015, 120, 47-51.	2.2	5
422	Relationship and Interconversion Between Superhydrophilicity, Underwater Superoleophilicity, Underwater Superaerophilicity, Superhydrophobicity, Underwater Superoleophobicity, and Underwater Superaerophobicity: A Mini-Review. Frontiers in Chemistry, 2020, 8, 828.	3.6	5
423	Tracking the interaction of drug molecules with individual mesoporous amorphous calcium phosphate/ATP nanocomposites – an X-ray spectromicroscopy study. Physical Chemistry Chemical Physics, 2020, 22, 13108-13117.	2.8	5
424	Fabrication of Three-Dimensional Microvalves of Internal Nested Structures Inside Fused Silica. Micromachines, 2021, 12, 43.	2.9	5
425	Laser Fabrication of Nanoholes on Silica through Surface Window Assisted Nano-Drilling (SWAN). Nanomaterials, 2021, 11, 3340.	4.1	5
426	Brittle–ductile transition in the PETG/PC blends by adding PTW elastomer. Polymers for Advanced Technologies, 2010, 21, 401-407.	3.2	4
427	Acidâ€modified carbon nanotubes distribution and mechanical enhancement in polystyrene/elastomer blends. Polymer Engineering and Science, 2012, 52, 964-971.	3.1	4
428	Kinetic study of a swelling-induced network of folds in a cross-linked PS-PDMS film. RSC Advances, 2015, 5, 3733-3742.	3.6	4
429	Locus-patterned sequence oriented enrichment for multi-dimensional gene analysis. Chemical Science, 2019, 10, 8421-8427.	7.4	4
430	Antibacterial silver-doped calcium phosphate synthesized by an enzymatic strategy for initial caries treatment. Ceramics International, 2020, 46, 22466-22473.	4.8	4
431	Bioorthogonal Chemical Signature Enabling Amplified Visualization of Cellular Oxidative Thymines. Analytical Chemistry, 2021, 93, 10495-10501.	6.5	4
432	Research on the technology of femtosecond laser micromachining based on image edge tracing. Science Bulletin, 2010, 55, 877-881.	1.7	3

#	Article	IF	CITATIONS
433	Microwave-assisted solvothermal ionic liquid rapid synthesis of aluminum fluorohydroxide single-crystalline octahedra. Materials Letters, 2013, 94, 104-107.	2.6	3
434	Fabrication of three-dimensional micro-Rogowski coil based on femtosecond laser micromachining. Applied Physics A: Materials Science and Processing, 2015, 120, 669-674.	2.3	3
435	Fano Resonance-Assisted Plasmonic Trapping of Nanoparticles. Plasmonics, 2017, 12, 627-630.	3.4	3
436	Hall of Fame Article: A Review of Femtosecond‣aserâ€Induced Underwater Superoleophobic Surfaces (Adv. Mater. Interfaces 7/2018). Advanced Materials Interfaces, 2018, 5, 1870033.	3.7	3
437	Flower-like calcium phosphoserine complex as biomimetic mineral with high bioactivity. Ceramics International, 2020, 46, 20914-20922.	4.8	3
438	Pairwise Proximityâ€Differentiated Visualization of Singleâ€Cell DNA Epigenetic Marks. Angewandte Chemie, 2021, 133, 3470-3474.	2.0	3
439	Underwater superpolymphobicity: Concept, achievement, and applications. Nano Select, 2021, 2, 1011-1022.	3.7	3
440	Theoretical Study on Symmetry-Broken Plasmonic Optical Tweezers for Heterogeneous Noble-Metal-Based Nano-Bowtie Antennas. Nanomaterials, 2021, 11, 759.	4.1	3
441	Fully Automatic Classification of Brain Atrophy on NCCT Images in Cerebral Small Vessel Disease: A Pilot Study Using Deep Learning Models. Frontiers in Neurology, 2022, 13, 846348.	2.4	3
442	Unusual rheological characteristics of polypropylene/organoclay nanocomposites in continuous cooling process. Journal of Applied Polymer Science, 2012, 125, E292.	2.6	2
443	Ultrafast optical Kerr gate of bismuth–plumbum oxide glass for time-gated ballistic imaging. Journal of Modern Optics, 2014, 61, 1452-1456.	1.3	2
444	A Förster Resonance Energy Transfer Ratiometric Probe Based on Quantum Dot-Cresyl Violet for Imaging Hydrogen Sulfide in Living Cells. Chinese Journal of Analytical Chemistry, 2018, 46, 39-47.	1.7	2
445	Property enhancement of poly(butylene) Tj ETQq1 1 0.784314 rgBT /Overlock 10 Tf 50 272 Td (succinate)/poly(via highâ€speed extrusion and <scp><i>in situ</i></scp> fibrillation. Journal of Applied Polymer Science, 2019. 136. 47549.	ethyleneg 2.6	lycolâ€≺scp> 2
446	Underwater Superoleophobic Tracks: Underwater Anisotropic 3D Superoleophobic Tracks Applied for the Directional Movement of Oil Droplets and the Microdroplets Reaction (Adv. Mater. Interfaces) Tj ETQq0 0 0 i	gB I. †Over	lock 10 Tf 50
447	Active Tuning of Hybrid Plasmonics in Graphene-Covered Metallic Nanotrench. Technical Physics Letters, 2020, 46, 526-531.	0.7	2
448	Rat model of cholelithiasis with human gallstones implanted in cholestasis-induced virtual gallbladder. World Journal of Methodology, 2016, 6, 154.	3.5	2
449	Addition–Elimination Mechanism-Activated Nucleotide Transition Sequencing for RNA Dynamics Profiling. Analytical Chemistry, 2021, 93, 13974-13980.	6.5	2
450	Facile oneâ€pot pyrolysis preparation of <scp>SnO₂</scp> / <scp>g ₃N₄</scp> composites for improved photocatalytic <scp>H₂</scp> production. Journal of Chemical Technology and Biotechnology, 2022, 97, 2921-2931.	3.2	2

#	Article	IF	CITATIONS
451	Superior Method for Measuring Chirp Structure of Femtosecond Supercontinuum Pulse. IEEE Photonics Technology Letters, 2013, 25, 261-263.	2.5	1
452	Pump power dependence of the spatial gating properties of femtosecond optical Kerr effect measurements. Applied Physics B: Lasers and Optics, 2013, 112, 279-283.	2.2	1
453	Fabrication and analytical evaluation of threeâ€dimensional microsolenoids achieved in fused silica by femtosecondâ€laserâ€based microsolidifying process. Micro and Nano Letters, 2013, 8, 623-628.	1.3	1
454	Inhibition of duck hepatitis B virus replication by mimic peptides in vitro. Experimental and Therapeutic Medicine, 2015, 10, 1697-1703.	1.8	1
455	Synthesis of polymerized calcium silicate hydrate nanostructures as drug carriers. Journal of Controlled Release, 2015, 213, e52.	9.9	1
456	Inferior vena cava segmentation with parameter propagation and graph cut. International Journal of Computer Assisted Radiology and Surgery, 2017, 12, 1481-1499.	2.8	1
457	Electrical and optical properties of metalâ€sandwiched ZnO/Ti/Cu/Ti/ZnO transparent conductive thin film. Micro and Nano Letters, 2018, 13, 1511-1515.	1.3	1
458	Bubble Passage: Underwater Superaerophobicity/Superaerophilicity and Unidirectional Bubble Passage Based on the Femtosecond Laser‣tructured Stainless Steel Mesh (Adv. Mater. Interfaces 14/2020). Advanced Materials Interfaces, 2020, 7, 2070077.	3.7	1
459	Facile Interfacial Synthesis of Densely Spiky Gold Nano-Chestnuts With Full Spectral Absorption for Photothermal Therapy. Frontiers in Bioengineering and Biotechnology, 2020, 8, 599040.	4.1	1
460	Synthesis of mesoporous manganese dioxide/expanded graphite composite and its lithium-storage performance. Bulletin of Materials Science, 2020, 43, 1.	1.7	1
461	Hydrogel-compartmentalized heterogeneous amplification for viral digital genotyping. Sensors and Actuators B: Chemical, 2022, 356, 131339.	7.8	1
462	Overexpression of phosphatidylethanolamine-binding protein 4 (PEBP4) associates with recurrence of meningiomas. Clinical Neurology and Neurosurgery, 2022, 214, 107148.	1.4	1
463	Platelet-Activating Biominerals Enhanced Injectable Hydrogels With Superior Bioactivity for Bone Regeneration. Frontiers in Bioengineering and Biotechnology, 2022, 10, 826855.	4.1	1
464	Fabrication of three-dimensional metallic microcomponents in fused silica by a femtosecond laser & micromoulding (FLM) method. , 2013, , .		0
465	Fidelity quantification of mercury(ii) ion via circumventing biothiols-induced sequestration in enzymatic amplification system. RSC Advances, 2016, 6, 80296-80301.	3.6	0
466	Dynamic near-field nanofocusing by V-shaped metal groove via a femtosecond laser excitation. Applied Physics A: Materials Science and Processing, 2016, 122, 1.	2.3	0
467	Manufacturing of functional polymer micro- and nano-structures by femtosecond laser pulse. , 2017, ,		0
468	Biomimic Nanominerals: Enzymatic Reaction Generates Biomimic Nanominerals with Superior Bioactivity (Small 51/2018). Small, 2018, 14, 1870250.	10.0	0

#	ARTICLE	IF	Citations
469	Temperature Sensor Based on Multimode Fiber Bragg Grating. , 2018, , .		0
470	Optical Properties of Metal Sandwiched ZnO/Ti/Cu/Ti/ZnO Thin Film. , 2018, , .		0
471	Coronavirus disease 2019: MRI examination procedures and infection prevention and protection. Annals of Translational Medicine, 2020, 8, 1074-1074.	1.7	0
472	IDDF2021-ABS-0154â€Selenium and mercury levels and the risk of non-alcoholic fatty liver disease (NAFLD): indications from the national health and nutrition examination survey (NHANES 2017–2018). , 2021, , .		0
473	Feng Chen's work on translational and clinical imaging. World Journal of Radiology, 2011, 3, 120.	1.1	0
474	High temperature high sensitivity optical fibre sensor based on multimode fibre Bragg grating. Micro and Nano Letters, 2018, 13, 1537-1541.	1.3	0
475	A bifunctional chemical signature enabling RNA 4-thiouridine enrichment sequencing with single-base resolution. Chemical Communications, 2022, 58, 1322-1325.	4.1	0